COBEM 2021 26th International Congress of Mechanical Engineering
November 22-26, 2021, Virtual Congress, Brazil
ABCM Associação Brasileira de Engenharia e Ciências Mecânicas

COB-2021-1440
INFLUENCE OF HEAT TREATMENTS AT 850, 900 AND 950 °C ON THE FORMATION OF SIGMA PHASE FOR UNS S32750 SUPER DUPLEX STAINLESS STEEL

Ernandes Marcos Scopel
Instituto Federal do Espírito Santo – Programa de Pós-Graduação em Tecnologia Sustentáveis
ernandes.scopel@ifes.edu.br

André Gustavo de Sousa Galdino
Instituto Federal do Espírito Santo – Programa de Pós-Graduação em Tecnologia Sustentáveis
andre.galdino@ifes.edu.br

Temistocles de Sousa Luz
Universidade Federal do Espírito Santo – Departamento de Engenharia Mecânica
temistocles.luz@icloud.com

Warlen Alves Monfardini
Instituto Federal do Espírito Santo – Coordenadoria do Curso de Engenharia Mecânica
warlen.monfardini@ifes.edu.br

Ricardo Salvador Boldrini
Instituto Federal do Espírito Santo – Programa de Pós-Graduação em Engenharia Metalúrgica e de Materiais
ricardo.boldrini@ifes.edu.br

Raquel Skíbina Verbeno
Instituto Federal do Espírito Santo – Graduação em Engenharia Mecânica
rsverbeno@gmail.com

Abstract. *Super duplex stainless steels (SDSS) are recognized because of their excellent mechanical properties and high corrosion resistance when compared to other steels. However, when these materials are subjected to temperatures from 400 to 1010 °C they can be affected with the presence of deleterious phases, such as chromium carbide. In many cases the presence of these phases can decrease some properties, especially corrosion resistance due to the protective layer deterioration. Therefore, this work aimed to analyze the sigma precipitation on UNS S32750 super duplex stainless steel after solubilization at 1125°C, aged at 850, 900 and 950°C for 10, 100 and 1000 min, quenched in water and also furnace cooled for samples aged at the three temperatures for 1000 min. Microhardness were measured to evaluate the influence of sigma phase precipitation. It was observed an increase of hardness with aging temperatures and aging times, with approximately 418 ± 4 HV0.5 for furnace cooled sample at 850°C for 1000 min. Yet, it is important to highlight that when investigating the precipitation of the sigma phase, a greater nucleation was observed at the interface of the austenite/ferrite phase, in the initial times of aging, the precipitation of the deleterious phases in finer grains contributed to the increase in hardness at 850 °C and with stabilization at 950 °C, because of the nucleation of larger grains, as a consequence of the increase in time and temperature of the treatment and also seen the intergranular precipitation in the ferritic stage of the sigma phase. These results collaborate to improve the understanding of sigma phase precipitation, in order to contribute to the choice of the appropriate parameters for the welding processes of the SDSS UNS S32750.*

Keywords: *super duplex stainless steel, phase transformation, aging, phase.*

1 INTRODUCTION

The technological development of new steel alloys, as well as the improvement of manufacturing techniques and their manufacturing processes, allowed the production of duplex stainless steels (DSS) and this must assume a prominent role in the industrial area. The application of super duplex stainless steel alloys (SDSS) covers an extensive industrial field, highlighting, for example, the sectors of the petrochemical industry, oil and gas exploration (onshore and offshore) and the chemical industry, since their properties of mechanical strength and corrosion resistance are much superior to common steels and other stainless steels.

SDSSs have a microstructure made up of balanced fractions of ferrite and austenite, in a proportion of approximately 50% each. This microstructural distribution allows steel to have the following characteristics or properties: high thermal conductivity, high tenacity, low coefficient of thermal expansion, good mechanical strength, considerable weldability, and especially corrosion resistance, especially pitting and crevice corrosion. Therefore, this steel is applied in several projects in the chemical-industrial environment, mainly because of the exceptional combination of mechanical properties and corrosion resistance (Hosseini *et al*., 2018a, 2018b, 2019; Zhang *et al*., 2017).

The most prevalent applications of SDSS occur in environments with high concentration of sodium chloride such as oil and gas pipelines, machinery for handling materials rich in chlorides and in storage vessels for the chemical industry and petrochemicals. Welding processes are used to manufacture pipelines, tanks and equipment, and the heat input used can change SDSS microstructures and their properties.

The importance of determining the mechanical properties and corrosion resistance of these alloys is highlighted, thus contributing to a better applicability of this material in manufacturing processes. Among the main challenges faced in the elaboration of special steels by researchers and manufacturers, the production of stainless steel with a low precipitation rate stands out which helps to minimize pitting corrosion. However, some phases, as: σ phase, χ phase, chromium carbides and nitrides, tend to form during welding (Kim *et al*., 2015). Several researches have been performed in the SDSS to obtain an ideal phase equilibrium and with the aim to observe the influence of these precipitates on the mechanical and electrochemical properties of these steels (Dandekar *et al.*, 2018; Devendranath Ramkumar *et al.*, 2015; Eghlimi *et al.*, 2015; Pérez *et al.*, 2016; Zhang *et al.*, 2016). These researches aimed to understand how these stages nucleate due to energy input from the manufacturing processes.

The nucleation of the sigma phase triggers a reduction in the mechanical properties and electrochemical resistance of the DSSs and SDSSs, causing punctual corrosion in areas adjacent to the precipitates, occurring mainly because it is a phase enriched in Cr and Mo. The influence of aging on the σ phase nucleation and growth is what provides the change from coral phase morphology to block with increasing treatment time and temperature. The importance of studying this behavior and phase characteristics can be observed in several studies (Chen; Weng; Yang, 2002; Hosseini *et al.*, 2018a; Li *et al.*, 2018; Ma *et al.*, 2017; Marques; Santos, 2016; Tavares *et al.*, 2018; Zhang *et al.*, 2016) and there are still questions to be answered about this topic.

This work aimed to investigate the influence of heat treatments at 850, 900 and 950 °C on the formation of the sigma phase in UNS S32750 superduplex stainless steel, using computational thermodynamics analysis, differential scanning calorimetry analysis and microstructural characterization.

Researches on this alloy has been designed over the years intending to develop improvements both in aspects relating to weldability properties, as well as corrosion resistance properties, in relation to the alloying elements present in this alloy. Therefore, this study contributes to the improvement of knowledge about the evolution of the phases of the SDSS UNS S32750, allowing the proper application of this alloy in industrial plants, and collaborating in the selection of appropriate parameters for the welding processes used in the manufacture and maintenance of these components.

2 MATERIALS AND METHODS

The UNS S32750 super duplex stainless steel sample used in this study was taken from a 406 mm diameter and 6 mm thick tube. Acquired by the Mechanical Engineering Department of the Federal University of Espírito Santo (UFES), through an agreement with a petrochemical company. To carry out studies of a research project that aims to analyze the effects of the action of oil and the environment saturated with sodium chloride on its mechanical properties and corrosion resistance. Three specimens of 15 x 15 x 6 mm^3 for each heat treatment temperature were used.

Chemical composition of as-received (AR) UNS S32750 SDSS was performed in an Oxford Foundry Master Pro Optical Emission Spectrometer. Results represent average chemical composition of three AR specimens, five measurements per specimen.

Differential Scanning Calorimetry (DSC) analysis was performed in a Netzsch STA 449 F3 Jupiter Simultaneous Thermal Analysis equipment using argon atmosphere with flow rate of 20mL/min. Solubilized sample was heated from 22 °C up to 1200 °C at 10 °C/min, and then cooled in the furnace down to room temperature.

By means of the chemical composition of the steel under study, identified by means of emission spectrometry analyses, Thermodynamic equilibrium state calculations were performed using the result of UNS 32750 SDSS using the FactSage® 7.2software with FSstel steel alloy® database.

The solubilization treatment (ST) and aging (A) thermal treatments were performed using a Fortelab MEZ 1700/4/E high-temperature furnace. Samples (ST1125/5) were solubilizided at 1125°C for 5 min and then cooled in water according to the Sandvik SAF 2507/13 standard. After solubilization, aging heat treatments samples were performed in order to provide transformation energy for the diffusion of the phases, which were nucleated in the microstructure, at temperatures of 850 °C, 900 °C and 950 °C, with holding time of 10, 100 and 1000 min per temperature, followed by cooling in water (WA850/10, WA850/100 and WA850/1000; WA900/10, WA900/100 and WA900/1000; WA950/10, WA950/100 and WA950/1000). Still, to analyze the evolution of the phases in another cooling media, another group of samples was aged at the same temperatures with holding time of 1000 min and cooled in the furnace (FA850/1000; FA900/1000 and FA950/1000).

These specimens were prepared and grinded for metallographic analysis according to ASTM E3-11 standard, polished in 1 μm alumina aqueous suspension, 1 μm and 0.25 μm diamond pastes followed by electrochemical attack using 30% KOH electrolyte solution with 2.5 V for 24 s, according to ASTM E407- 07.

Optical micrography (OM) was performed using an Olympus CX31 RTSF optical microscope to analyze ferrite/austenite proportions and morphologies, besides the precipitates and deleterious phases. Scannin Electron Microscopy with Energy-Dispesive X-ray Spectroscopy (SEM/EDS) analyzes were performed in a TESCAN VEGA3 with an Oxford X-MaxN, operating at 30.0 kV and 110 μA. X-ray diffractography analysis (XRD)was performed using a Bruker D8 Discover diffractometer, using Co-kα radiation source (λ = 1.78901 Å), with the following settings: 35 kV and 40 mA, observation range or $25 \leq 2\theta \leq 120°$, 0.02° step with exposure time of 2.0 s for each step.

Microhardness tests were performed according to ASTM E384-17 using a Mitutoyo HM-12 microhardness tester. Image J® v. 1.52n was used to quantify the phase fractions, to measure the mean area of the precipitates and the circularity of the precipitates in the micrographs according to ASTM E562-19.

3 RESULTS AND DISCUSSIONS

3.1 CHEMICAL COMPOSITION

Table 1 shows the chemical composition of UNS 32750 SDSS. Comparing the chemical composition of the sample obtained through optical emission spectrometry with chemical composition stabilished by ASTM A789/A789M-20, it is possible to see that the sample used is an UNS 32750 SDSS.

Table 1 – Results of UNS 32750 SDSS chemical composition.

Chemical element	Chemical composition – ST (wt%)	Chemical composition (wt%) (ASTM A 789/A 789M -01a)
Fe	Balance	Balance
C	0.02	0.03 max
Si	0.44	0.8 max
Mn	0.88	1.20 max
P	0.018	0.035 max
S	0.001	0.020 max
Cr	24.6	24.0 – 26.0
Mo	3.4	3.0 – 5.0
Ni	6.4	6.0 – 8.0
Cu	0.29	0.50 max
N	0.26	0.24 – 0.32

As it can be seen, the steel used in this work is a super duplex stainless steel, as can be seen in other works such as those by Gunn (2003), Gupta *et al.* (2018), Hosseini *et al.* (2018b) and Tavares *et al.* (2018).

3.2 COMPUTATIONAL THERMODYNAMIC ANALYSIS

Results of Table 1 were used for thermocomputational simulations, via FactSage® 7.2 to predict phases that can nucleate at 850 °C, 900 °C and 950 °C and simulation results are presented in Fig. 1.

For the temperature range from 850°C up to 950°C, there are ferrite (δ) and austenite (γ) phases and intermetallic sigma (σ) phase and chromium nitride (Cr_2N), both of them are deleterious phases; σ phase precipitates by cooling from 890°C up to approximately 440°C as result of δ phase decomposition at high temperatures while Cr_2N precipitates by cooling from 950°C up to 400°C it usually happens at the grain boundaries, that is, at the interface between the δ/δ, δ/γ and γ/γ phases, and also inside the ferrite grains (Hosseini *et al*., 2018b; Zhang *et al*., 2017). These deleterious phases decrease UNS 32570 SDSS corrosion resistance and other mechanical properties (such as toughness and ductility). It is also verified that in the range of temperature from 1025 °C and 1125 °C (heat treatment for UNS 32750 according to ASTM A 790/A 790/M-20) there are only ferrite and austenite phases, with 50% of each phase at 1035 °C (Berecz *et al.*, 2015; Hosseini *et al.*, 2018c; Pérez *et al.*, 2016; Hatwig *et al*., 2014; Zhang *et al*., 2017; Zhang *et al*., 2018; Maamache et al., 2021; Zhu *et al.*, 2021).

Still observing Fig. 1, it can be observed that at 850 °C, there is 32.5% ferrite, 54% austenite, 8.5% sigma phase and 3.9% chromium nitride. However, it is noted that at 900 °C the sigma phase dissolved in the ferritic matrix and then the fractions of the phases at this temperature are approximately 46% ferrite, 51.5% austenite and 2.5% nitride of chrome. At 950 °C, the system tends to phase equilibrium, with only the two primary stages of this alloy remaining at this temperature, with 49% ferrite and 51% austenite, as shown by Hosseini et al. (2018c), Ma et al. (2017) and Maamache et al. (2021).

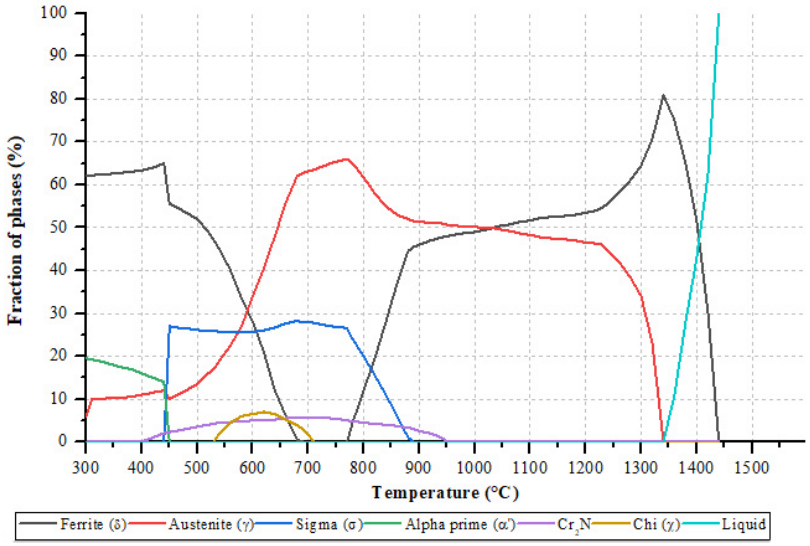

Figure 1 – Simulation of phase evolution in SDSS UNS S32750.

3.3 DIFFERENTIAL EXPLORATORY CALORIMETRY (DSC)

Figure 2 shows the curve generated in the DSC analysis for UNS S32750 SDSS. During the heating cycle, it was possible to identify 5 peaks of endothermic transformations, which were analyzed in parallel with the thermocomputational simulation, shown in Figure 1, thus making it tangible to identify the precipitated precipitated phase in that particular peak.

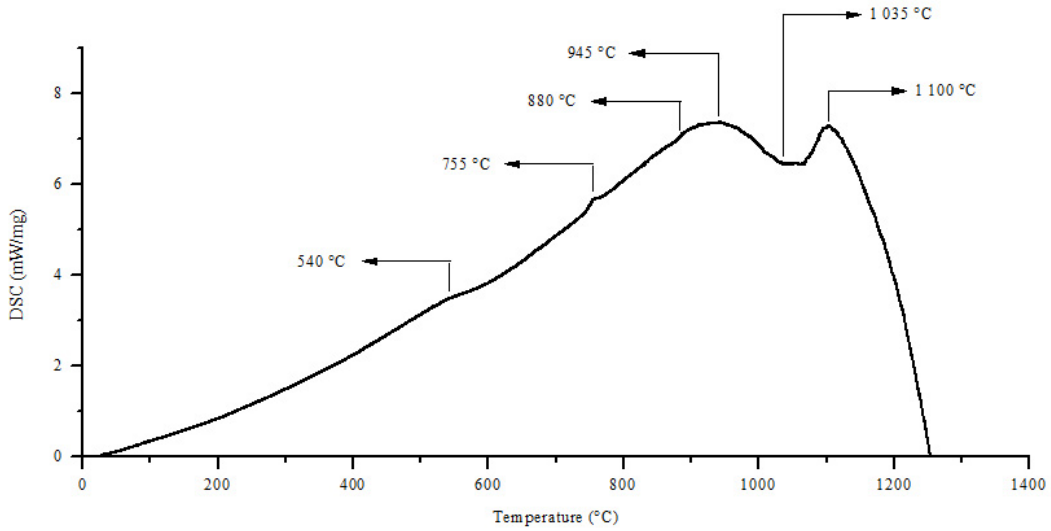

Figure 2 – DSC curve of SDSS UNS S32750

The first endothermic peak occurs at 540 °C, whose enthalpy of reaction of 3.500 J/g represents the nucleation of the χ phase, a precipitate rich in molybdenum, demonstrating the similarity with the results observed in previous works, with a small difference in the enthalpy of reaction (Berecz *et al*., 2015, 2020; Khoshnaw *et al.*, 2021). The second endothermic peak shows an enthalpy of reaction of 5.698 J/g, with a temperature of 755 °C, referring to the transformation of the sigma and austenite phase into a ferrite phase (Haghdadi *et al.*, 2018; Hosseini *et al.*, 2018b; Shamanth; Ravishankar; Hemanth, 2019).

At 880 °C, the third endothermic peak that was observed presents 7.038 J/g of reaction enthalpy, which can be associated with the complete transformation of the sigma phase and the threshold of the search for the equilibrium point of the two primary phases (ferrite/austenite), exhibiting compliance with the results seen in the DSC analysis of previous works (Berecz *et al.*, 2015, 2020; Khoshnaw *et al.*, 2021; Tahchieva; Llorca-Isern; Cabrera, 2019)

The fourth endothermic peak was verified at approximately 945 °C, with an enthalpy of reaction in the order of 7.345 J/g, referring to the complete dissolution of chromium nitride in the primary matrix of the alloy, according to the

correlation in the thermocomputational simulation, the same peak was observed in previous works (Berecz et al., 2015, 2020; Khoshnaw *et al.*, 2021). The third and fourth ones are located in the temperature range studied in this research. And the last endothermic peak, at 1100 °C and with an enthalpy of reaction of 7.302 J/g, which is related to the transformation of austenite into the ferrite phase (Berecz *et al.*, 2015; Hao *et al.*, 2020; Steiner Petrovič *et al.*, 2012; Tahchieva; Llorca-Isern; Cabrera, 2019)

By comparing the outcomes of the thermocomputer simulation and the thermal analysis by DSC, it was possible to emphasise an aspect in the temperature of 1035 °C, where the enthalpy of reaction of 6.480 J/g, which is associated with the equilibrium of the ferritic and austenitic phases, with approximately 50 %p of each phase, also observed in other researches (Berecz *et al.*, 2020; Khoshnaw *et al.*, 2021). Another point of discussion is the last peak at 1100 °C in the DSC analysis, which can be correlated in the thermal simulation, with the smooth decline of the austenite volume fraction from approximately 1080 °C, due to the dissolution process of the austenitic phase in the ferritic phase. Furthermore, according to the analysis in FactSage®, a severe transformation of the austenitic phase was seen, from 1225 °C, with greater transformation kinetics for the δ phase, a point of similarity as stressed in previous works (Hosseini *et al*., 2018c; Zhang *et al.*, 2017a, 2018).

3.4 MICROSTRUCTURAL CHARACTERIZATION

Optical micrographs of UNS 32750 SDSS of AR, ST1125/5, WA950/10 and WA950/1000 are presented in Fig. 3.

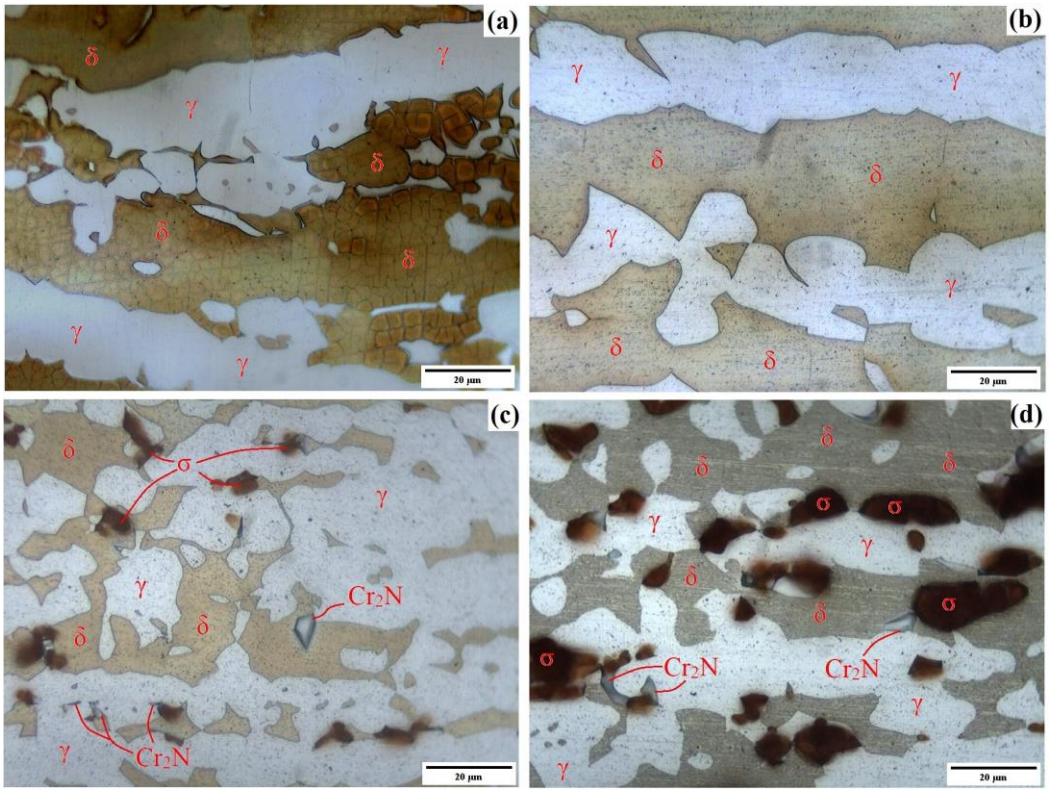

Figure 3 – Optical micrographs of UNS S32750 SDSS: (a) AR; (b) ST1125/5; (c) WA950/10; (d) WA950/100. 30% KOH etchant, 1,000X.

AR and ST1125/5 samples presented ferrite/austenite in stable proportions (dark regions – ferrite; light regions – austenite). Fig 3(a) shows the duplex microstructure with ferrite grains well refined, as a result from cold deformation process of UNS 32750 SDSS sample. During the solubilization treatment, these grains were submitted to stress relief and coalescence of refined grains that resulted in formation of larger grains of the respective phases (Fig. 3(b)).

In Fig. 3(b) it can also be observed that light austenite grains are separated islands in the ferrite matrix, and despite of having some larger grains, from a global perspective of the distribution of γ phase in the micrographs, the microstructure presents lamellar-shaped grains that follows rolling direction irregular edges contours (Nilsson, 1992; Nilsson *et al.*, 2000; Padilha; Rios, 2002).

It is also possible to notice that increasing the aging remaining time there was an increase in the nucleation of sigma phase, as well as chromium nitride precipitation, in spite of the results of thermodynamics simulation (Figure 1) and of DSC (Figure 2) that had shown that sigma phase would already be dissolved in ferrite matrix and Cr_2N would not precipitate at 950°C. Concerning aging remaining time, one can seen a few σ phase fraction had nucleated in the γ/α phase

boundary, decreasing δ phase for WA950/10 sample (Fig. 3(c)). For WA950/100 (Fig. 3(d)), sigma phase content increased from ferrite comsuption. For WA950/1000 sample, all ferrite phase was comsumed by sigma phase development, involving γ phase grains (Ma *et al.*, 2017).

SEM micrographs of ST1125/5, WA950/1000 and WA900/10 are presented in Fig. 4. One could observe that σ phase nucleation and the intergranular conditions in the grain boundary, and also the interface of δ/γ phases. In Fig. 5(a) it is noted that no precipitate is identified, different from what is seen in Fig. 5(b), in which there are several points with this feature due to alloy elements with higher atomic weight present in the UNS 32750 SDSS (Hernández-Trujillo *et al.*, 2021; Maamache *et al.*, 2021; Shamanth, Ravishankar and Hemanth, 2019).

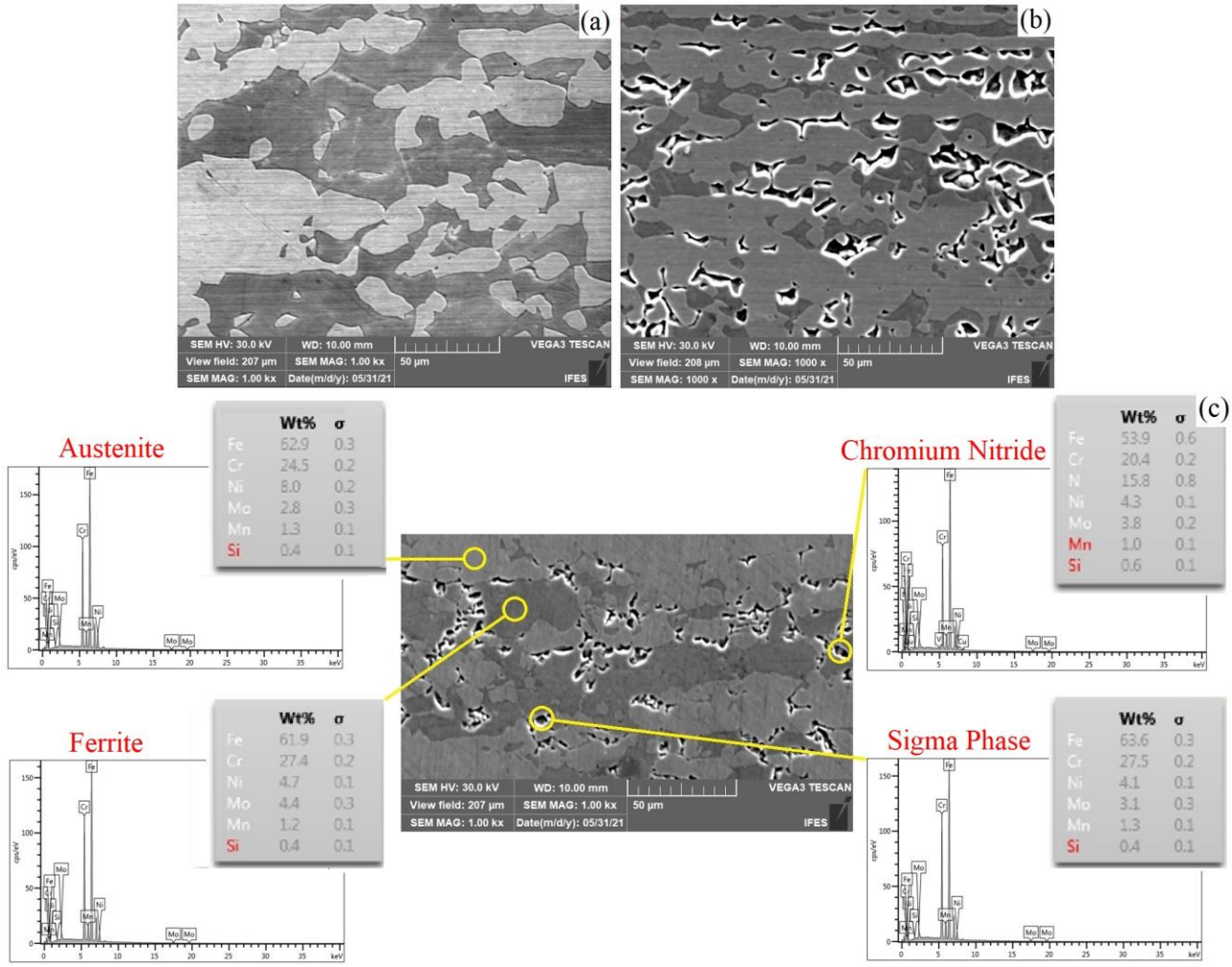

Figure 4 – Micrograph of samples: (a) ST1125/5; (b) WA950/1000; (c) and EDS of WA900/10.

It can be seen in Fig. 4(c) both the primary and the secondary phases that had their nucleation in WA900/10 sample; for the primary phases, γ phase has high nickel content (gammagenic element), while δ is enriched with chromium (alphagenic element) (Nilsson, 1992; Padilha; Rios, 2002; Pardal *et al.*, 2010). For the secondary phases, σ phase has high chromium and low molybdenum contents, while chromium nitrides present high chromium and nitrogen contents, which nitrogen is noticed in nitrides due to its high content. Nevertheless, EDS is a semiquantitative technique and no quantification can be used by this technique. These observations of elementary compositions are in agreement with previous studies (Hao *et al.*, 2020; Hernández-Trujillo *et al.*, 2021; Maamache *et al.*, 2021).

3.5 X-RAY DIFFRACTION (DRX) OF SAMPLES

Fig. 5 shows XRD diffractions of samples with different aging treatment (water or furnace cooling) at different times (10, 100 and 1000 min) compared to ST1125/5 sample.

For AR and ST1125/5 samples, it is observed that only δ and γ phases peaks can be seen, with δ peaks presenting intensity slightly superior of γ phase peaks due to the absence of precipitates as σ phase, carbide, nitrides or secondary

phases to decompose δ phase, as seen in the diffractograms of all samples after aging treatment at 850 °C (Dandekar *et al.*, 2018; Tandon *et al.*, 2018).

At 850 °C δ phase peaks have low intensity while the σ and γ peaks increases their intensity when compared to diffractograms of AR and ST samples. This confirms again that the conceptualization already presented in several studies, in which they demonstrate that σ phase nucleation directly depends on the solid-state transformation of $\delta \rightarrow \gamma + \sigma$ (Hosseini *et al.*, 2018c; Li *et al.*, 2019; Ma *et al.*, 2017).

XRD diffractograms of AR, ST1125/5, WA850/10, WA850/100, WA850/1000 and FA850/1000 samples are shown in Fig. 6 presents phases and precipitates.

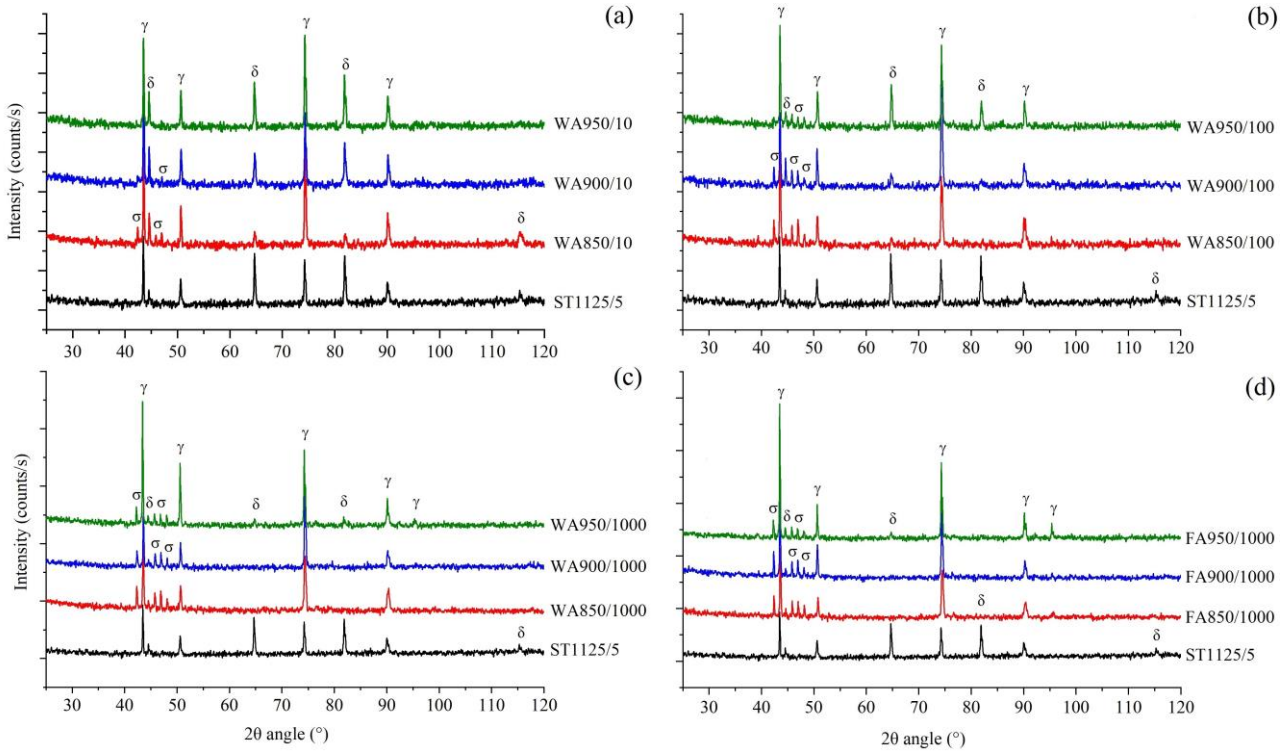

Figure 5 – XRD diffractograms of: (a) ST1125/5, WA850/10, WA900/10, WA950/10; (b) ST1125/5, WA850/100, WA900/100, WA950/100; (c) ST1125/5, WA850/1000, WA900/1000, WA950/1000; (d) ST1125/5, FA850/1000, FA900/1000, FA950/1000 samples.

It is possible to notice that the longer the time, the higher the increase of the σ phase peak s intensity, with decrease of δ phase peaks until all δ phase comsuption by σ phase as previously observed in Fig. 3 and Fig. 4. For γ phase, peaks did not demonstrate significant changes, highlighting that at 95.7° there was an increase in its intensity for FA950/1000 sample (Gennari *et al.*, 2020; Maamache *et al.*, 2021; Núñez *et al.*, 2020).

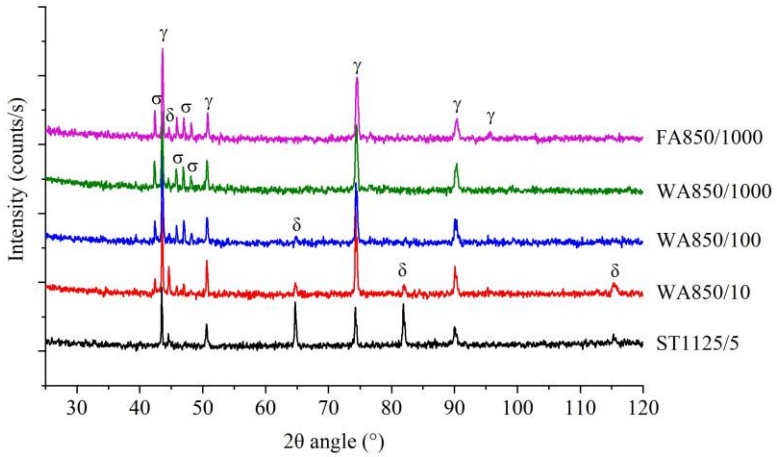

Figure 6 – XRD diffractograms of ST1125/5, WA850/10, WA850/100, WA850/1000 and FA850/1000 samples.

For WA samples after 1000 min of remaining time, σ phase consumed almost all δ phase as one can see in Fig. 5(c). Same behavior was noted by Gennari *et al.* (2020); Hosseini *et al.* (2018c) and Kumar *et al.* (2017).

3.6 MECHANICAL VICKERS MICRODUTURE TESTS

Microhardness of samples are presented in Fig. 7. Comparing microhardness of AR and ST1125/5 samples, it can be verified that there is a slight decrease of microhardness. Opposite behavior is were observed when samples are aging treated in water as time goes by with maximum microhardness for FA850/1000 (Fig. 7(a); Fig. 7(b)). Those results are similar to those of Hosseini et al. (2018a, 2018b) and Berecz et al. (2015).

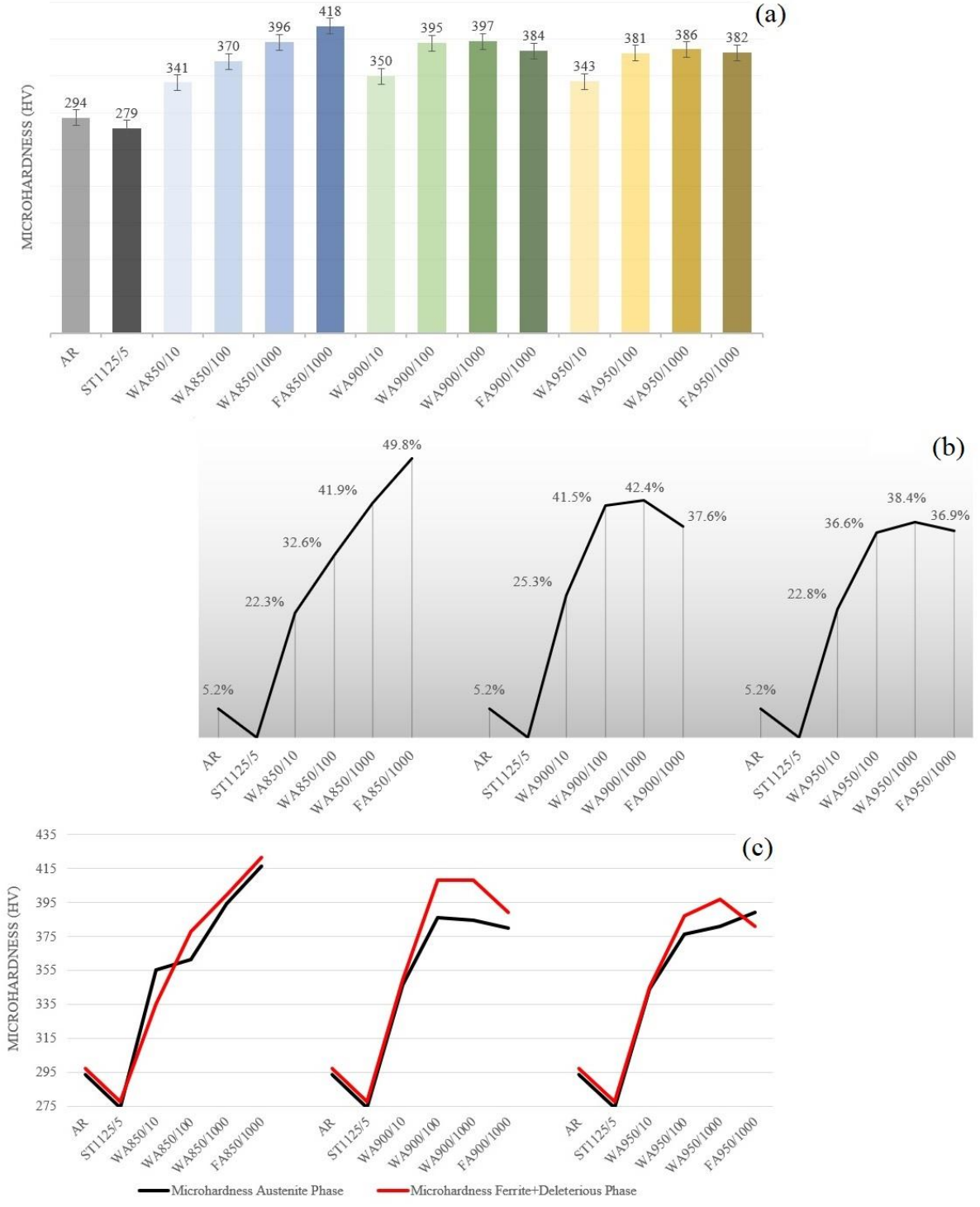

Figure 7 – (a) Microhardness of UNS 32750 SDSS samples; (b) Evolution of microhardness; (c) Microhardness of phases.

For samples treated at 900°C, there was a slight increase of microhardness with the increase of aging time for those samples that were water cooled; however, when sample was cooled inside the furnace. The same behavior was observed for samples treated at 950°C (Fig. 7(a); Fig. 7(b)). All aging treated samples presented microhardness higher than those of AR and ST1125/5 (Berecz *et al.*, 2015; Dandekar *et al.*, 2018; Hosseini *et al.*, 2018b, 2018c).

For microhardness showed in Fig. 7(c), it was not possible to measure the microhardness of δ phase without σ phase and Cr_2N. The microhardness of the γ phase with the solubilization treatment had an average value of 274 ± 7 (0.05), and remained approximately stable when subjected to the aging process at 900 °C and 950 °C for 100 and 1000 min, regardless of the cooling method (Gennari *et al.*, 2020; Hosseini *et al.*, 2018c; Kumar *et al.*, 2017). This similar behavior is noticed for microhardness of samples aged for 850 °C, 900 °C and 950 °C for 10 min, i. e., microhardness remains stable between 344 and 355 HV(0.05).

By analyzing the microhardness of δ phase, one can conclude that the microhardness of this phase in the solubilized condition presents an average value of 278 ± 10 HV(0.05); maximum microhardness is observed for FA850/1000 sample, reaching 422 ± 3 HV(0.05), which shows the influence of the interaction of σ and Cr_2N phases in the increase of microhardness for this steel, since for this aging temperature it is still within the nucleation range of the sigma phase, and the furnace cooling collaborates to yield a greater amount of energy for the transformation and nucleation of the deleterious phases in the alloy, as underscored by Gennari *et al.* (2020), Hosseini *et al.* (2018c), Li *et al.* (2019), Nilsson (1992), Tahchieva, Llorca-Isern, Cabrera (2019), and Zhang *et al.* (2018).

4 CONCLUSIONS

In this work, the evolution of phases for UNS S32750 SDSS in the conditions: AR, ST1125/5, WA850/10, WA850/100, WA850/1000, FA850/1000, WA900/10, WA900/100, WA900/1000, FA900/1000, WA950/10, WA950/100, WA950/1000, FA950/1000 were investigated. From these results, we can conclude that:

• Computational thermodynamic analysis using FactSage® 7.2 software did not allow predicting sigma phase precipitation at 900 °C and 950 °C that were observed in samples heat treated under the conditions of this work by microscopy (optical and scanning electron) and diffraction X-rays, since the software used does not parameterize the aging treatment, it only simulates phase transformations in thermodynamic equilibrium. However, it was possible to predict chromium nitride in the temperature range of 400 °C to approximately 950 °C.

• It was possible to identify, more precisely, the formation of sigma and chromium nitride phases by DSC, whose results were corroborated when compared with the results of microscopy (optical and scanning electrons) and X-ray diffraction, with a slight difference when compared to computer simulation (945 °C for DSC results and approximately 950 °C for computer simulation).

• Precipitation of the σ phase is strongly affected by aging time, in the temperature range studied, as a result of increased secondary phase precipitation with greater decomposition of the ferritic phase at 850 °C, followed by samples treated at 900 °C.

• In the early stages of aging, the precipitation behavior of the σ phase in the SDSS UNS S32750 is governed by the transformation mechanism of the eutectoid decomposition of the $\delta \rightarrow \sigma + \gamma 2$ phase, so that the main nucleation region of this deleterious phase was the interface of γ/δ phases. With advancing aging time, intergranular nucleation of the ferritic phase can be observed.

• Finally, an almost linear growth was observed in the microhardness of the samples heat-treated at 850 °C, having the solubilized samples as its starting point, and then, it was found in the TEF 850/1000 sample, the highest surface microhardness with 418 ± 4 HV(0.5), and for the microhardness of the phases, both the austenitic with 416 ± 2 HV(0.05) and the ferritic+deleterian phase with 422 ± 3 HV(0.05).

AKNOWLEDGEMENTS

The authors would like to thank the teams of the Materials and Reduction and Ceramics Laboratories of IFES and the team of LABPETRO of UFES for their support in the development of this research.

5 REFERENCES

Amercian Society for Testing anda Matetials, "*ASTM A790 / A790M-20: Standard Specification for Seamless and Welded Ferritic/Austenitic Stainless Steel Pip*e" (West Conshohocken, Philadephia: ASTM International, 2020), p. 1–10.

———, "*ASTM E3-11: Standard Practice for Preparation of Metallographic Specimens*" (West Conshohocken, Philadephia: ASTM International, 2011), p. 1–12.

———, "*ASTM E384-17: Standard Test Method for Microindentation Hardness of Materials*" (West Conshohocken, Philadephia: ASTM International, 2017), p. 1–40.

———, "*ASTM E407-07: Standard Practice for Microetching Metals and Alloys*" (West Conshohocken, Philadephia: ASTM International, 2007), p. 1–21.

———, "*ASTM E562-19: Standard Test Method for Determining Volume Fraction by Systematic Manual Point Count*" (West Conshohocken, Philadephia: ASTM International, 2019), p. 1–7.

Berecz, Tibor, Éva Fazakas, Eniko Réka Fábián, Péter Jenei, e János Endre Maróti, *"Investigation of thermally induced deterioration processes in cold worked SAF 2507 type duplex stainless steel by DTA"*, Crystals, 10.103390 (2020), 1–11.

Berecz, Tibor, Éva Fazakas, István Mészáros, and István Sajó, "*Decomposition Kinetics of Ferrite in Isothermally Aged SAF 2507-Type Duplex Stainless Steel*", Journal of Materials Engineering and Performance, 24.12 (2015), 4777–88.

Chen, T. H., K. L. Weng, and J. R. Yang, "*The effect of high-temperature exposure on the microstructural stability and toughness property in a 2205 duplex stainless steel*", Materials Science and Engineering A, 338.1–2 (2002), 259–70.

Dandekar, Tushar Ramdas, Aman Gupta, Amit Kumar, Rajesh Kisni Khatirkar, and Basavaraj Vadavadagi, "*Shielded metal arc welding of UNS S32750 steel: Microstructure, mechanical properties and corrosion behaviour*", Materials Research Express, 5.10 (2018), 1–13.

Devendranath Ramkumar, K., Anshuman Singh, Shubham Raghuvanshi, Ankur Bajpai, Tathagat Solanki, M. Arivarasu, et al., "*Metallurgical and mechanical characterization of dissimilar welds of austenitic stainless steel and super-duplex stainless steel - A comparative study*", Journal of Manufacturing Processes, 19 (2015), 212–32.

Eghlimi, Abbas, Morteza Shamanian, Masoomeh Eskandarian, Azam Zabolian, and Jerzy A. Szpunar, "*Characterization of microstructure and texture across dissimilar super duplex/austenitic stainless steel weldment joint by austenitic filler metal*", Materials Characterization, 106.1 (2015), 27–35.

Gunn, R. N. *Duplex Stainless steels. Microestructure, properties and applications*. 1ª Edição ed. Cambridge, England: Abington Publishing, 2003.

Gupta, Aman, Amit Kumar, T Baskaran, Shashi Bhushan Arya, Rajesh Kisni Khatirkar. *Effect of Heat Input on Microstructure and Corrosion Behavior of Duplex Stainless Steel Shielded Metal Arc Welds*. Transactions of the Indian Institute of Metals, [s. l.], v. 71, n. 7, p. 1595–1606, 2018.

Gennari, Claudio, Luca Pezzato, Gianmarco Tarabotti, Andrea Zambon, Andrea Di Schino, and Irene Calliari, "*Influence of electropulsing treatments on mechanical properties of UNS S32750 duplex stainless steel*", Materials, 13.7 (2020), 1–18.

Haghdadi, N., P. Cizek, P. D. Hodgson, V. Tari, G. S. Rohrer, and H. Beladi, "*Effect of ferrite-to-austenite phase transformation path on the interface crystallographic character distributions in a duplex stainless steel*", Acta Materialia, 145.1 (2018), 196–209.

Hao, Yansen, Jian Li, Xin Li, Wanchun Liu, Guangming Cao, Chenggang Li, et al., "*Influences of cooling rates on solidification and segregation characteristics of Fe-Cr-Ni-Mo-N super austenitic stainless steel*", Journal of Materials Processing Tech. journal, 275.116326 (2020), 1–9.

Hatwig, Rodrigo Afonso, Nestor Cezar Heck, Alexandre da Silva Rocha, and Luciano Aparecido Kempski, "*Characterization of Super Duplex Steel phases through thermodynamic-computational simulation* (in Portuguese)", in 69° ABM Annual Congress (São Paulo - SP / Brasil, 2014), p. 1680–87.

Hernández-Trujillo, Saúl Leonardo, Victor Hugo Lopez-Morelos, Marco Arturo García-Rentería, Rafael García-Hernández, Alberto Ruiz, and Francisco Fernando Curiel-López, "*Microstructure and fatigue behavior of 2205/316l stainless steel dissimilar welded joints*", Metals, 11.93 (2021), 1–18.

Hosseini, Vahid A., Kjell Hurtig, Daniel Eyzop, Agneta Östberg, Paul Janiak, and Leif Karlsson, "*Ferrite content measurement in super duplex stainless steel welds*", Welding in the World, 63.2 (2019), 551–63.

Hosseini, Vahid A., Leif Karlsson, Sten Wessman, and Nuria Fuertes, "*Effect of sigma phase morphology on the degradation of properties in a super duplex stainless steel*", Materials, 11.6 (2018a), 933–46.

Hosseini, Vahid A., Leif Karlsson, Cem Örnek, Pierfranco Reccagni, Sten Wessman, and Dirk Engelberg, "*Microstructure and functionality of a uniquely graded super duplex stainless steel designed by a novel arc heat treatment method*", Materials Characterization, 139.1 (2018b), 390–400.

Hosseini, Vahid A., Leif Karlsson, Dirk Engelberg, and Sten Wessman, "*Time-temperature-precipitation and property diagrams for super duplex stainless steel weld metals*", Welding in the World, 62.3 (2018c), 517–33.

Khoshnaw, Fuad, Cornelia Marinescu, Ancuta Sofronia, Cornel Munteanu, Maria Marcu, Laura Eugenia Barbulescu, et al., "*Microstructural and thermoanalytical characterization of super duplex stainless steel - UNS S32760-F55*", Materials Today Communications, 28.102644 (2021), 1–11.

Kim, Hye Jin, Soon Hyeok Jeon, Soon Tae Kim, e Yong Soo Park, "*Influence of the shielding gas composition on the passive film and erosion corrosion of tube-to-tube sheet welds of hyper duplex stainless steel*", Corrosion Science, 91 (2015), 140–50.

Kumar, Amit, Rajesh Kisni Khatirkar, Darshan Chalapathi, Gulshan Kumar, and Satyam Suwas, "*Microstructure and Texture Development during Cold Rolling in UNS S32205 and UNS S32760 Duplex Stainless Steels*", Metallurgical and Materials Transactions A: Physical Metallurgy and Materials Science, 48.5 (2017), 2349–62.

Li, J., C. W. Du, Z. Y. Liu, X. G. Li, and M. Liu, "*Effect of microstructure on the corrosion resistance of 2205 duplex stainless steel. Part 1: Microstructure evolution during isothermal aging at 850 °C and evaluation of anticorrosion*

properties by methods of cyclic potentiodynamic polarization and electr", Construction and Building Materials, 189.1 (2018), 1286–93.

Li, Jian-sin, Guan-ju Cheng, Hung-wei Yen, Liberty T Wu, Yo-lun Yang, Rudder T Wu, et al., "*Thermal cycling induced stress – assisted sigma phase formation in super duplex stainless steel*", Materials & Design, 182.108003 (2019), 1–13.

Liu, Heping, Hu'er Sun, Bin Liu, Dazhao Li, Fenger Sun, and Yongtao Zhang, "*Analysis of χ phase precipitation in aged 2205 duplex stainless steel*", Journal Wuhan University of Technology, Materials Science Edition, 30.3 (2015), 591–95.

Ma, M, H Ding, R D K Misra, Z Y Tang, H B Li, and G W Fan, "*A study on precipitation kinetics of sigma phase in a hot-rolled super duplex stainless steel during isothermal aging based on the Johnson – Mehl – Avrami model*", Ironmaking and Steelmaking, 44.4 (2017), 311–19.

Maamache, Bouzid, Billel Cheniti, Brahim Belkessa, Karima Tahar-chaouch, and Ramdhane Kouba, "*Effect of Aging Temperature on the Microstructure, Local Mechanical Properties, and Wear Behavior of a UNS S32750 Super Duplex Stainless Steel*", Journal of Materials Engineering and Performance, 30.1 (2021), 546–55.

Marques, I. J., and T. F. A. Santos, "*Precipitation Kinetics of Detrimental Intermetallic Phases in Duplex Stainless Steel UNS S32205* (in Portuguese)", in 22° CBECiMat - Brazilian Congress of Engineering and Materials Science (Natal - RN / Brasil, 2016), p. 5349–61.

Nilsson, J. O., "*Super duplex stainless steels*", Materials Science and Technology (United Kingdom), 8.1 (1992), 685–700.

Nilsson, J. O., P. Kangas, T Karlsson, and A. Wilson, "*Mechanical properties, microstructural stability and kinetics of sigma-Phase Formation in 29Cr-6Ni-2Mo-0.38N Superduplex Stainless Steel*", Metallurgical and Materials Transactions A, 31.1 (2000), 35–45.

Núñez, Yamid, Marcio Mafra, Rigoberto E. Morales, Paulo César Borges, and Giuseppe Pintaude, "*The effect of plasma nitriding on the synergism between wear and corrosion of SAF 2205 duplex stainless steel*", Industrial Lubrication and Tribology, 72.9 (2020), 1117–22.

Padilha, A. F., and P. R. Rios, "*Decomposition of austenite in austenitic stainless steels*", ISIJ International, 42.4 (2002), 325–37.

Pardal, Juan Manuel, Sérgio Souto Maior Tavares, Maria da Penha Cindra Fonseca, José Adailson de Souza, Lorena Menezes Vieira, and Hamilton Ferreira Gomes de Abreu, "*Deleterious phases precipitation on superduplex stainless steel UNS S32750:Characterization by light optical and scanning electron microscopy*", Materials Research, 13.3 (2010), 401–7.

Pérez, Argelia Fabiola Miranda, Marco Breda, Irene Calliari, Gladys Yerania Pérez Medina, and Rolf Sandström, "*Detrimental Cr-rich Phases Precipitation on SAF 2205 Duplex Stainless Steels Welds After Heat Treatment*", Soldagem & Inspeção, 21.2 (2016), 165–71.

SANDVIK MATERIALS TECHNOLOGY, "*Sandvik SAF 2507 - Strip steel*" (Sandviken, Sweden: Sandvik AB, 2013), p. 7 <http://www.smt.sandvik.com/zh-cn/materials-center/material-datasheets/billets/sandvik-saf-2507/>

Shamanth, V., K. S. Ravishankar, and K. Hemanth, "*Duplex Stainless Steels: Effect of Reversion Heat Treatment*", in Stainless Steels and Alloys (IntechOpen, 2019), I, 71.

Steiner Petrovič, Darja, Miran Pirnat, Grega Klančnik, Primož Mrvar, and Jožef Medved, "*The effect of cooling rate on the solidification and microstructure evolution in duplex stainless steel: A DSC study*", Journal of Thermal Analysis and Calorimetry, 109.3 (2012), 1185–91.

Tahchieva, Alisiya Biserova, Núria Llorca-Isern, and José María Cabrera, "*Duplex and superduplex stainless steels: Microstructure and property evolution by surface modification processes*", Metals, 9.3 (2019).

Tandon, Vipin, Awanikumar P. Patil, Ramesh C. Rathod, and Sourabh Shukla, "*Influence of cold work on electrochemical behavior of 316L ASS in PEMFC environment*", Materials Research Express, 5.2 (2018).

Tavares, S. S.M., J. M. Pardal, B. B. Almeida, M. T. Mendes, J. L.F. Freire, and A. C. Vidal, "*Failure of superduplex stainless steel flange due to inadequate microstructure and fabrication process*", Engineering Failure Analysis, 84.August 2017 (2018), 1–10.

Zhang, Binbin, Zhouhua Jiang, Huabing Li, Shucai Zhang, Hao Feng, and Heng Li, "*Precipitation behavior and phase transformation of hyper duplex stainless steel UNS S32707 at nose temperature*", Materials Characterization, 129.1 (2017), 31–39.

Zhang, Ziying, Huizhen Zhang, Jun Hu, Xiaoxiao Qi, Yang Bian, Ao Shen, et al., "*Microstructure evolution and mechanical properties of briefly heat-treated SAF 2507 super duplex stainless steel welds*", Construction and Building Materials, 168 (2018), 338–45.

Zhang, Ziying, Huizhen Zhang, Hui Zhao, and Jin Li, "*Effect of prolonged thermal cycles on the pitting corrosion resistance of a newly developed LDX 2404 lean duplex stainless steel*", Corrosion Science, 103 (2016), 189–95.

Zhu, M., F. He, Y. F. Yuan, S. M. Yin, S. Y. Guo and J. Pan. "*Effect of Aging Time on the Microstructure and Corrosion Behavior of 2507 Super Duplex Stainless Steel in Simulated Marine Environment*", Journal of Materials Engineering and Performance, 1059-9495, (2021), 1 – 15.